Dynamic control of an accelerometer bandwidth through tunable damping factor and effective moment of inertia

B. Fain, F. Souchon, A. Berthelot, R. Anciant, P. Robert, G. Jourdan

DYNAMIC CONTROL OF AN ACCELEROMETER BANDWIDTH THROUGH TUNABLE DAMPING FACTOR AND EFFECTIVE MOMENT OF INERTIA

B. Fain, F. Souchon, A. Berthelot, R. Anciant, P. Robert and G. Jourdan*
Univ. Grenoble Alpes, F-38000 Grenoble, France
CEA, LETI, MINATEC Campus, F-38054 Grenoble, France

ABSTRACT

In this paper, we report the dynamic bandwidth control of an accelerometer by reducing both its quality factor and its effective inertia. The MEMS is coupled with two built-in resistors to tune the frequency response through a DC voltage. The conception, the fabrication and the electrical testing of the accelerometer are presented. The reduction of the effective moment of inertia is experimentally evidenced on the basis of an analytical model. To the best of our knowledge, such a control of the bandwidth including inertial effects has not been reported yet. This strategy does not impact the quasi-static gain of the device and may be operated in vacuum.

INTRODUCTION

The mechanical behavior of a MEMS may be modified by a proper coupling with dedicated electronics [1]. Compared to approaches based on viscous effects [2-3], this enables the dynamic control of the MEMS response, possibly at the price of some additional complexity. For instance, an accelerometer driven with a signal proportional to the seismic mass speed has been proposed in order to increase the damping of the structure [4]. More frequently, the mechanical stiffness may be tuned through a simple DC voltage by electrical trimming [5-6]. An approach based on ohmic losses has also been proposed to tune the damping coefficient of silicon carbide nanowire resonators [7] or that of an accelerometer [8]. In this latter work, the quality factor was decreased by about 5 at 10^{-2} mbar.

In this paper, we show that this type of electrostatic feedback may also be employed to add a negative contribution to the inertia of a resonator. For this purpose, the coupling between the inertial mass of an accelerometer and resistors is enhanced by an appropriate design. The resistors are integrated within the device to minimize the impact of parasitic capacitances. The reduction of the effective inertial mass is experimentally evidenced. In addition, the modification of inertia is exploited to increase the device bandwidth.

DESIGN

The device is based on a rotating structure with piezoresistive detection (M&NEMS concept) such as that described in ref. [9] (Fig. 1). The movement of the large inertial mass induces a stress within the two nanogauges located close to the hinge at the center of the structure. Compared with previous works, two additional structures located on the edge of the seismic mass form two variable capacitors to ensure the electromechanical coupling. Each of them is composed of ten radial comb structures made of hundred interdigitated fingers electrodes. The variation of capacitance is achieved through surface variation to keep the balance between the two electrostatic forces when displacement occurs. Each structure is connected with an undoped nanoscale nanowire which is used as a built-in resistor of typically 50 MΩ. A voltage V_{EM} is applied on the other resistor's output to control the electromechanical response of the device. When an acceleration is applied, MEMS motion generates a motional current in the capacitance circuit, what results in a voltage drop across the resistors and a feedback torque on the seismic mass. Note that the two structures are symmetric, so that the resulting torque is zero if there is no motion.

The mechanical behavior of the structure without electromechanical coupling ($V_{EM} = 0$) was simulated using Comsol Multiphysics. The natural frequency is expected at 1023 Hz. The coupling was designed through an analytical approach.

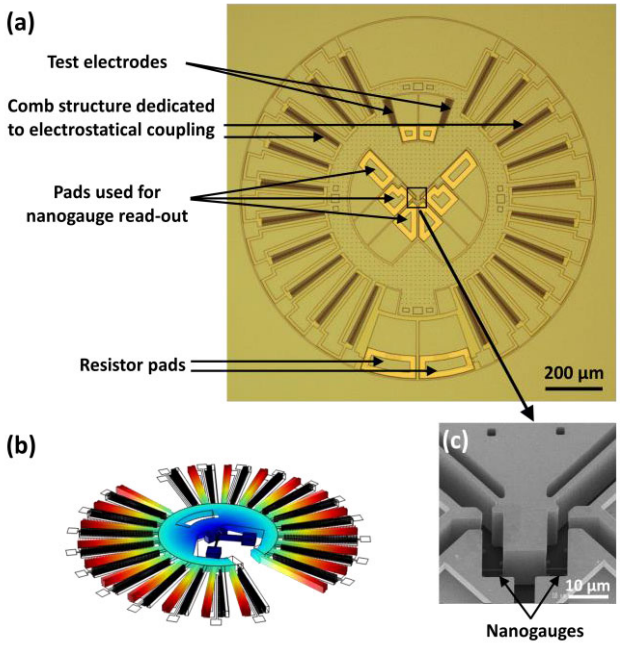

Figure 1: (a) optical picture of the linear accelerometer. The electrodes at the edge of the seismic mass are dedicated to electrostatic coupling with dissipative resistors. The resistors are located below the resistor pads. (b) Orthoradial displacement field of the first mode (Natural frequency: 1023 Hz) simulated using Comsol Multiphysics. (c) SEM picture of the nanogauges located at the center of the structure that ensure differential piezoresistive detection

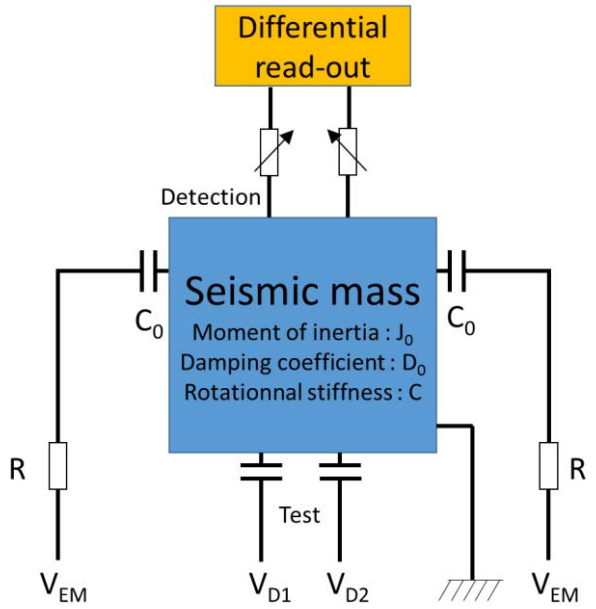

Figure 2: Scheme of the electronic circuit connecting the seismic mass to polarization V_{EM} through the two electrodes and resistors

The angular movement of the inertial mass is described by the following equations, using notations of Figure 2.

$$J_0\ddot{\theta} + D_0\dot{\theta} + C\theta = M_{ext} + M_{el} \quad (1)$$

M_{el} is the electrostatic torque and M_{ext} accounts for any other efforts applied to the center of rotation of the structure, such as a torque resulting from inertial forces or actuation through test electrodes.

M_{el} is the sum of two components, M_{el1} and M_{el2}, corresponding respectively to the torques induced by the two structures on the two sides of the device. M_{el1} depends on the voltage drop across the resistance. For small angular displacement, the electromechanical torque is approached by a development in first order in current and can be related to the variations of the charge Q on the capacitance and the parameter $C' = \frac{\partial C_0}{\partial \theta}$.

$$M_{el1} = \frac{1}{2} C'(V_{EM}^2 - 2 * RQj\omega) \quad (2)$$

The small charge variations δQ is linked to the angular displacement:

$$\delta Q = V_0 \frac{\delta C_0}{1+RC_0\, j\omega} = V_0 \frac{C'\delta\theta}{1+R^2 C_0^2 \omega^2}(1 - RC_0 j\omega) \quad (3)$$

Combining equation (2) and (3) in the time domain, it comes:

$$M_{el1} = \frac{1}{2} C' V_0^2 - \frac{D_{el}}{2}\dot{\theta} + \frac{J_{el}}{2}\ddot{\theta} \quad (4)$$

With :

$$D_{el} \approx 2 * RC'^2 V_0^2 \quad (5)$$

$$J_{el} = RC_0 * D_{el} \approx 2 * R^2 C_0 C'^2 V_0^2 \quad (6)$$

As a result, the electrostatic torque can be described as

$$M_{el} = -D_{el}\dot{\theta} + J_{el}\ddot{\theta} \quad (7)$$

It appears that the electrostatic effort is composed of two terms, respectively proportional to the first and the second derivative of the angular displacement. The MEMS oscillator is well described by a standard oscillator with an effective moment of inertia $J = J_0 - J_{el}$ and an effective damping coefficient $D = D_0 + D_{el}$:

$$(J_0 - J_{el})\ddot{\theta} + (D_0 + D_{el})\dot{\theta} + C\theta = M_{ext} \quad (8)$$

FABRICATION

The MEMS is fabricated using 200mm standard MEMS technologies, based on a process flow similar to that of ref. [9] as described in Figure 3. The process starts from a SOI wafer (a). As a first step, the silicon top layer is processed to define the nanogauges doped with boron ($N_A = 5.10^{19}$) and undoped nanowires (b). A 21-µm thick silicon layer is then grown to form the MEMS part of the device (c). The mobile part is patterned and then released by a HF vapor process (d). A cap wafer, including a sealing ring and two interconnexion levels, is sealed on top of the first wafer by Au/Si eutectic bonding (e).

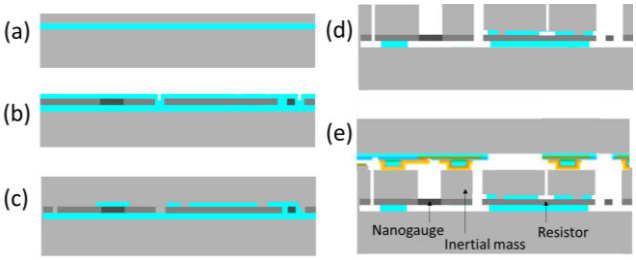

Figure 3: Main steps of the process flow. (a) SOI wafer; (b) silicon top layer patterning and protection by silicon dioxide; (c) epitaxy; (d) HF vapor release; (e) eutectic bonding

RESULTS

The frequency response of the MEMS before wafer-level packaging was experimentally measured at 1 mbar using the test electrodes and standard lock-in technique as a function of the polarization V_{EM} on the 500 – 1250 Hz frequency range (Fig. 4). Without electromechanical coupling ($V_{EM} = 0$), the accelerometer presents a resonance at 994 Hz with a quality factor of 105. When V_{EM} is applied, the MEMS response reveals an upwards shift of the resonance. This shift cannot be explained by electrostatic non-linearities (i.e. negative stiffness) or decrease of the quality factor, that both tends to decrease the resonant frequency. A decrease of the inertia of the device is more likely to explain the MEMS behavior.

The accurate determination of the natural frequency and the quality factor for each measurement is achieved by appropriate fitting and plotted in Figure 5. Assuming that the rotational stiffness is not impacted by the capacitance stiffness of the surface variation based capacitances related

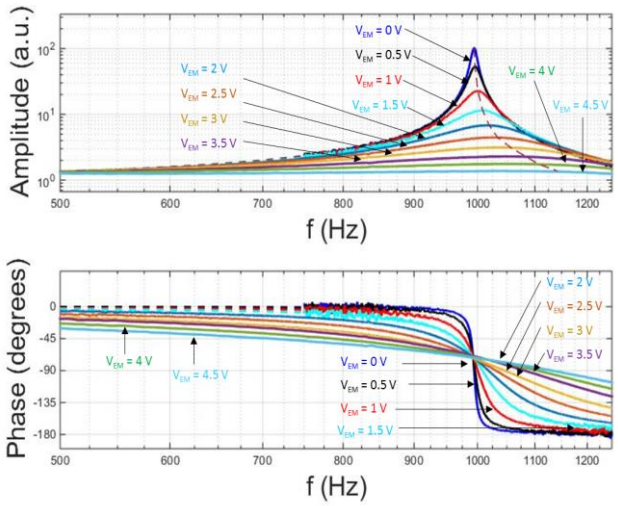

Figure 4: Frequency response of the accelerometer as a function of V_{EM}, measured at 1 mbar (continuous line) and related data fitting (dashed line). The shift of the resonant frequency is plotted in dashed line as a guide for the eye.

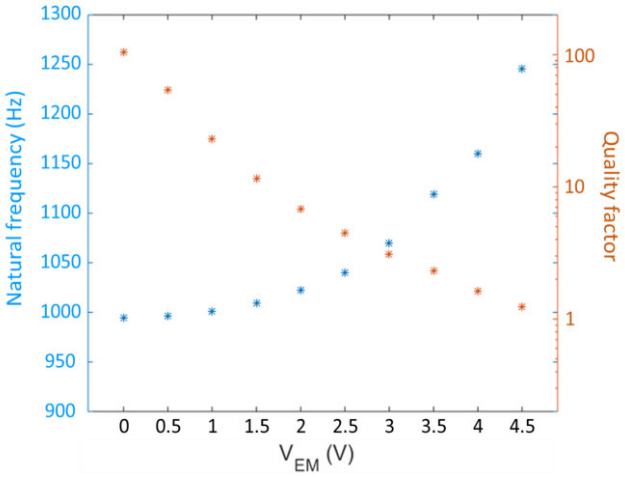

Figure 5: Natural frequency and quality factor versus V_{EM}

to process imperfections, one can deduce from these measurements the relative modification of the effective inertia and that of the damping coefficient through the following equations:

$$\frac{J(V_{EM})}{J(V_{EM}=0)} = \frac{f_0^2(V_{EM}=0)}{f_0^2(V_{EM})} \quad (9)$$

$$\frac{D(V_{EM})}{D(V_{EM}=0)} = \frac{(f_0 Q)(V_{EM}=0)}{(f_0 Q)(V_{EM})} \quad (10)$$

The results are plotted in Figure 6. The experimental data are in good agreement with a fit based on equations (5-6) and allows to recover numerical values of the main MEMS parameters (Table 1).

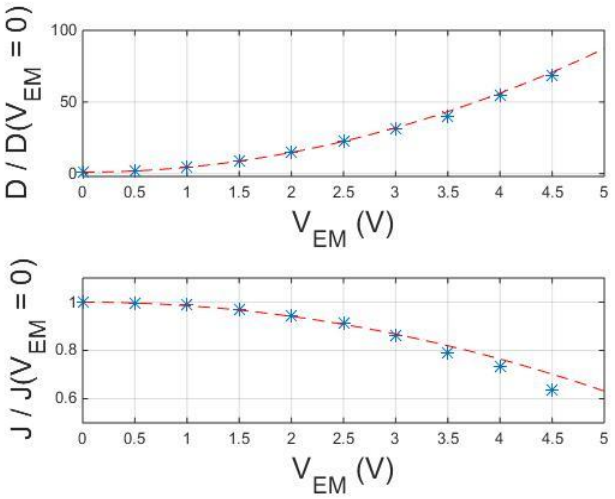

Figure 6: Dependence of the damping factor D (a) and the moment of inertia J (b) to the polarization V_{EM}. The fit with the analytical model is plotted in dashed red line.

The characteristics inferred from the experimental measurements are used to determine the bandwidth of the accelerometer, presented in Figure 7. The bandwidth is defined either by the + 3 dB cut-off frequency below the frequency resonance if the device presents a resonance higher than 3 dB or by the - 3 dB cut-off frequency above the frequency resonance otherwise. At $V_{EM} = 4.5V$, the quality factor is 1.25 and the bandwidth is expected at 1706 Hz. This reflects the combination of two effects. First, the decrease of the quality factor below 1.4, what leads to a jump of 250% of the bandwidth that occurs between 4 and 4.5 V in Figure 7. Second, the increase of the natural frequency related to the decrease of the effective inertia of the device. As a whole, the bandwidth is increased up to 316% when compared to the initial bandwidth of 538 Hz.

Table 1: Estimation of the main MEMS parameters

Parameter	Value
C	$5{,}9.10^{8}$ N.m
J_0	$1{,}5.10^{15}$ kg.m²
D_0 (1 mbar)	$8{,}9.10^{-14}$ N.m.s
RC_0	71,8 µs
C_0	1,32 pF
R	54 MΩ

DISCUSSION

We investigate here the issue concerning the stability of the device. At a sufficiently high value of V_{EM}, the effective inertia should be negative, hence the inertial mass is expected to rapidly move to the maximal allowed displacement, set by mechanical stops. As a matter of facts, measurements achieved at $V_{EM} > 4.5V$ (not shown) are likely to end up in that way.

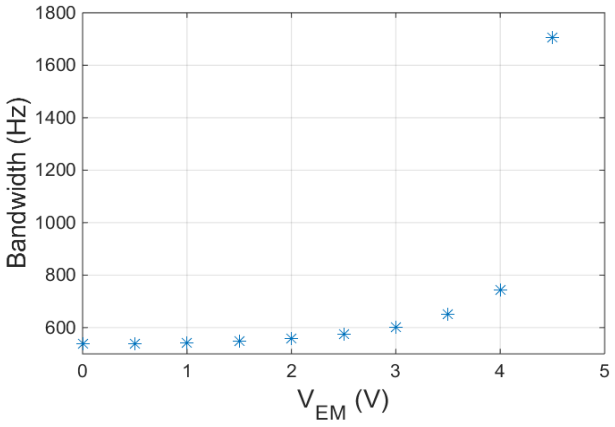

Figure 7: MEMS bandwidth vs V_{EM}. The bandwidth is defined either by the + 3 dB cut-off frequency below the frequency resonance if the device presents a resonance higher than 3 dB or by the - 3 dB cut-off frequency above the frequency resonance otherwise.

Interestingly, for $V_{EM} \leq 7V$, the MEMS can still be operated if an additional actuation voltage is added to one of the test electrode. We therefore believe that the moment of inertia of the device is still positive and that the failure of the device is related to more common electrostatic effects. Most probably, the static effort imposed by each of the two structures devoted to electromechanical coupling does not balance adequately because of a small discrepancy between the two structures. The impact of such mismatch is enhanced by the high voltage V_{EM} applied to both structures and results in pull-in phenomenon. These effects can be corrected by the additional actuation. For $V_{EM} > 7V$, such a strategy does not seem to be sufficient to recover a satisfactory operating point.

One can deduce from equation (6) that instability is expected at a critical voltage V_{EM}^{c} :

$$V_{EM}^{c} = \sqrt{\frac{J_0}{2 * R^2 C_0 C'^2}} \qquad (11)$$

V_{EM}^{c} is estimated at 8.2 V. The instability observed above 7V is therefore attributed to a negative effective moment of inertia rather than pull-in instability.

CONCLUSION

In this paper, the impact of electrostatic coupling on the inertia of a M&NEMS accelerometer is evidenced. The upwards shift of the resonant frequency of the accelerometer is observed and explained by an analytical model. The results comply with the theoretical expectations and demonstrate that the moment of inertia may be decreased by 36%. The modification of inertia is employed in combination with the related decrease of the quality factor to increase the bandwidth of the accelerometer by 316%, from 538 Hz to 1706 Hz.

Interestingly, the reduction of inertia does not impact the MEMS behavior at low frequency. First, the quasi-static gain of the device is not affected, unlike any strategy based on a modification of the device stiffness. Second, there is no additional thermomechanical noise related to the reduction of inertia, though the related damping effects does increase the thermomechanical noise.

We also point out the limitations of such approach, i.e. the instability phenomenon that arises when V_{EM} is increased. In this case, the reduction of the inertial mass may be detrimental to the behavior of the device. For instance, the further decrease of the quality factor would be limited by the stability issue. To prevent such effects to occur, the inertia of the device may be increased.

REFERENCES

[1] S. O. R. Moheimani, "A survey of recent innovations in vibration damping and control using shunted piezoelectric transducers," *IEEE Transactions on Control Systems Technology*, vol. 11, no. 4, pp. 482–494, Jul. 2003.

[2] P. W. Barth, F. Pourahmadi, R. Mayer, J. Poydock, and K. Petersen, "A monolithic silicon accelerometer with integral air damping and overrange protection," in *IEEE Technical Digest on Solid-State Sensor and Actuator Workshop*, 1988, pp. 35–38.

[3] B. Fain, A. Chaehoi, A. Berthelot, T. Verdot, F. Souchon, S. Delachanal, A. Koumela, A. Nowodzinski, H. Lhermet, G. Jourdan, P. Rey and P. Robert, "High-damped accelerometer based on squeeze-film damping and piezoresistive nanogauge detection for vibrating environments," in *2017 19th International Conference on Solid-State Sensors, Actuators and Microsystems (TRANSDUCERS)*, 2017, pp. 603–606.

[4] S. Marco, J. Samitier, O. Ruiz, A. Herms, and J.R. Morante, "Analysis of electrostatic-damped piezoresistive silicon accelerometers," *Sensors and Actuators A: Physical*, vol. 37–38, no. Supplement C, pp. 317–322, 1993.

[5] J. J. Yao and N. C. MacDonald, "A micromachined, single-crystal silicon, tunable resonator," *Journal of Micromechanics and Microengineering*, vol. 5, no. 3, p. 257, 1995.

[6] I. Y. Park, C. W. Lee, H. S. Jang, Y. S. Oh, and B. J. Ha, "Capacitive sensing type surface micromachined silicon accelerometer with a stiffness tuning capability," in *Proceedings MEMS 98. IEEE.*

[7] T. Barois *et al.*, "Ohmic electromechanical dissipation in nanomechanical cantilevers," *Phys. Rev. B*, vol. 85, no. 7, p. 75407, Feb. 2012.

[8] Y. Deimerly, P. Rey, P. Robert, T. Bourouina, and G. Jourdan, "Electromechanical damping in MEMS accelerometers: A way towards single chip gyrometer accelerometer co-integration," in *2014 IEEE 27th International Conference on Micro Electro Mechanical Systems (MEMS)*, 2014, pp. 725–728.

[9] P. Robert, V. Nguyen, S. Hentz, L. Duraffourg, G. Jourdan, J. Arcamone and S. Harrison, "M&NEMS: A new approach for ultra-low cost 3D inertial sensor," in *2009 IEEE Sensors*, 2009, pp. 963–966.

CONTACT

B. Fain, bruno.fain@cea.fr